

A detail preserving variational model for image Retinex[☆]

Zhihao Gu^a, Fang Li^{a,*}, Xiao-Guang Lv^b



^aSchool of Mathematical Science and Shanghai Key Laboratory of PMMP, East China Normal University, Shanghai, China

^bSchool of Science, Huaihai Institute of Technology, Lianyungang, Jiangsu, China

ARTICLE INFO

Article history:

Received 16 July 2018

Revised 2 November 2018

Accepted 29 November 2018

Available online 7 December 2018

Keywords:

Retinex

Reflectance

Illumination

Variational model

Image decomposition

ABSTRACT

In this paper, we propose a detail preserving variational model for Retinex to simultaneously estimate the illumination and the reflectance from an observed image. Most previous models use the log-transform as pretreatment which results in loss of details in reflectance. From this observation, a detail preserving variational method is proposed for better decomposition. Different from the log-transform based models, the proposed model performs the decomposition directly in the image domain. Mathematically, we prove the existence of a solution for the proposed model. Numerically, we derive an efficient iterative algorithm by utilizing alternating direction method of multipliers (ADMM) method. Experimental results demonstrate the effectiveness of the proposed method. Compared with other closely related Retinex methods, the proposed method achieves competitive results on both subjective and objective assessments.

© 2018 Elsevier Inc. All rights reserved.

1. Introduction

The idea of Retinex was first introduced by Land and McCann [1] to model the perception of human vision and the purpose of the Retinex theory is to decompose an observed image as the product of the illumination and the reflectance. In such a decomposition, removing the illumination effects of the lighting becomes possible.

As we know, recovering both illumination and reflectance from an observed image is a mathematically ill-posed problem [1] and various methods were then proposed to solve this problem. Path-based algorithms were proposed by Land and McCann [1–3] and further studied in [4–7]. Partial differential equations (PDE) based methods were proposed by Horn [8] in 1974 and developed in [9]. Kimmel et al. [10] proposed a variational framework to estimate the illumination and used an efficient multi-resolution algorithm to solve the model. They assumed the smoothness of the illumination but had no priors of the reflectance included in the model. Ma et al. [11] introduced a total variation (TV) and nonlocal TV regularized model which was solved by Bregman iteration for Retinex theory. They further established an L_1 -based variational model [12] for Retinex which is solved by a fast computational approach. Ng et al. [13] studied and developed a TV model for Retinex which also considered the reflectance in the model. However, the reflectance image obtained from Retinex was usually an over-enhanced image [13] because of the log-transform. Wang et al. [14] defined the model as a constrained optimization problem associated with the deduced energy functional and solved the problem with an alternating minimization scheme. Lan et al. [15] proposed a spatially adaptive Retinex variational model for the uneven intensity correction of remote sensing

* This research is supported by the National Natural Science Foundation of China (NSFC) (Nos. 61731009, 11671002), Science and Technology Commission of Shanghai Municipality (No. 18dz2271000), and Nature Science Foundation of Jiangsu Province (No. BK20181483).

* Corresponding author.

E-mail address: fli@math.ecnu.edu.cn (F. Li).

images. Spatial information was used to constrain the TV regularization strength of the reflectance. The split Bregman optimization algorithm was used to solve the model. Liang et al. [16] proposed a convex variational model which can effectively decompose the gradient field of images into salient edges and relatively smoother illumination field through the first- and second- order total variation regularization. A primal-dual splitting method was introduced to solve the model. Fu et al. [17] showed that the log-transform was not ideal for the decomposition and proposed a new weighted variational model for better prior representation which was imposed in the regularization terms for Retinex. An alternating minimization scheme was adopted to solve the proposed model. Park et al. [18] proposed a low-light image enhancement method using the variational-optimization-based Retinex algorithm in the image domain. However, in their model, it is required that the illumination should be close to an estimated illumination given by performing gamma correction on the given images which seems not suitable.

Most of the existing variational models perform a log-transform on the original image in their models to turn the product form into the addition form. This operation can reduce the computational complexity and simulate the human eye perception of light intensity [17]. However, Fu et al. [17] pointed out that the log-transform enlarges the variation of gradient magnitude in dark regions and may lead to an undesirable result like loss of finer details in the estimated reflectance. So they added weights into the regularization terms to eliminate the effects of log-transform to some extent.

The main drawback of the log-transform based models is the loss of details, especially in high-intensity regions. To overcome this drawback, in this paper, we propose a detail preserving variational model for Retinex to estimate the reflectance with fine details and smooth illumination simultaneously. An efficient algorithm is designed to solve the proposed model based on the alternating direction method of multipliers (ADMM) method. Experimental results and comparisons demonstrate the effectiveness of the proposed model. Our main contributions are: (1) we propose a new constrained variational model for image Retinex; (2) we prove the existence of a minimizer of the proposed model; (3) we derive an efficient algorithm and give the convergence analysis.

The paper is organized as follows. In Section 2, we present the proposed model along with some theoretical analysis about the existence of the solution. In Section 3, we introduce an effective iterative algorithm to solve the proposed model and study the convergence of the algorithm. In Section 4, we present the numerical results. Finally, concluding remarks are given in Section 5.

2. Model and minimizer

2.1. Motivation

The primary goal of Retinex theory is to decompose an observed image I into two different images, the reflectance R and the illumination L , such that

$$I(x, y) = R(x, y)L(x, y) \quad (1)$$

at each point (x, y) in the image domain. Estimating R and L is an ill-posed problem. In order to overcome the ill-posedness, lots of variational models with various priors are proposed. In most existing variational models, the log-transform is first performed on Eq. (1) in the image domain to get

$$i = r + l \quad (2)$$

in the logarithmic domain, where $i = \log(I)$, $r = \log(R)$ and $l = \log(L)$. Then the problem becomes estimating r and l respectively.

However, as pointed out in [17], log-transform leads to serious distortion of gradient information. As we know

$$\nabla r = \nabla \log(R) = \frac{1}{R} \nabla R. \quad (3)$$

Therefore, we have

$$|\nabla r| \rightarrow 0 (R \rightarrow +\infty), \quad |\nabla r| \rightarrow \infty (R \rightarrow 0). \quad (4)$$

It is obvious that $|\nabla r|$ in the low reflectance areas will become very large, while $|\nabla r|$ in the high reflectance areas will become very small.

Fig. 1 demonstrates this property of log-transform. Fig. 1(a) is the test image which has a dark background and bright foreground. Fig. 1(b) shows the log-transformed image, in which the dark regions are enhanced while the bright regions are over enhanced. Fig. 1(c) and (d) shows the magnitude of the gradient corresponding to Fig. 1(a) and (b), respectively. Compared Fig. 1(c) and (d), it is obvious that after log-transform, in the dark regions the magnitude of gradient becomes very strong while in the bright regions it becomes very weak. Hence, the conventional regularization term such as total variation emphasizes too much on the dark region and cannot keep a good balance for different regions. This may lead to the loss of details in the reflectance component, especially in bright regions.

2.2. Model

To overcome the drawback of log-transform in image Retinex, we propose to decompose the image directly without using log-transform. Our basic assumptions are as follows:

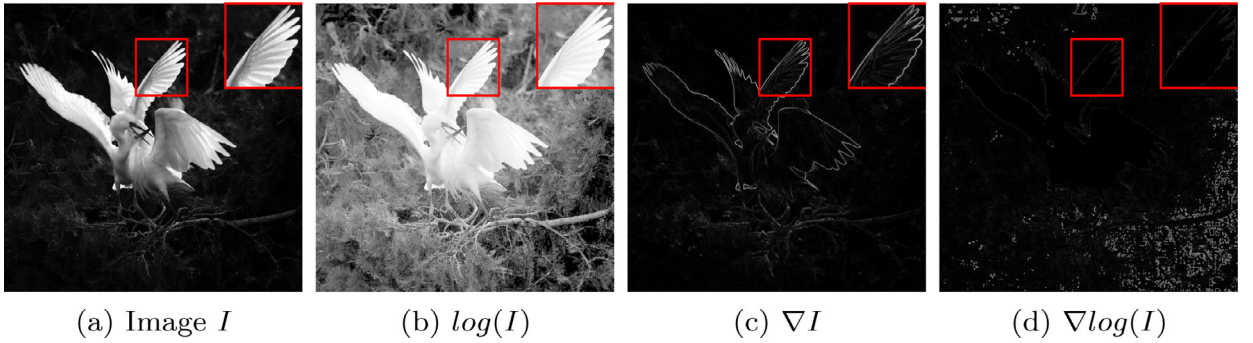


Fig. 1. Drawback of the log-transform.

- The illumination L is spatially smooth.
- The reflectance R is piecewise constant.
- R and L satisfy the constraints: $0 < \tau \leq R \leq 1$ and $L \geq I$.

Based on the above assumptions, we propose the following variational model:

$$\begin{aligned} E(R, L) = & \frac{1}{2} \int_{\Omega} |R \cdot L - I|^2 dx + \lambda_1 \int_{\Omega} |\nabla R| dx + \frac{\lambda_2}{2} \int_{\Omega} |\nabla L|^2 dx, \\ \text{s.t. } & \tau \leq R \leq 1, \quad I \leq L, \end{aligned} \quad (5)$$

where λ_1 and λ_2 are positive parameters. In the proposed model, the first term is an L_2 data fidelity term which forces a proximity between I and the product of the estimated R and L . The second term is the total variation regularization term which enforces that R is piecewise constant. The third term is the H^1 regularization term which enforces the spatial smoothness on L .

We note that the first and the second assumptions are widely used in image Retinex. The third assumption is different in the lower bound of R . The conventional lower bound of R is zero while in our assumption it is $\tau > 0$. This variation is for the purpose of mathematical analysis in the next subsection. Actually, $R \geq \tau$ is also reasonable since it is hard for any material to reach zero reflectance.

Note that the three terms in our model (5) also appear in the model of [18]. However, there are some differences between the two models. Firstly, our model is a constrained model while that of [18] is an unconstrained one. The constraints bring benefits for both theoretical analysis and numerical effectiveness. Secondly, the model of [18] has an additional fidelity term involving a pre-estimation of illumination which is not exact, while our model estimates both reflectance and illumination automatically.

It is easy to write down the log-transform version of the proposed model (5):

$$\begin{aligned} \min_{r, l} & \frac{1}{2} \int_{\Omega} |r + l - i|^2 dx + \lambda_1 \int_{\Omega} |\nabla r| dx + \frac{\lambda_2}{2} \int_{\Omega} |\nabla l|^2 dx, \\ \text{s.t. } & -\infty < r \leq 0, \quad i \leq l. \end{aligned} \quad (6)$$

Note that (6) is equivalent to the model considered in [13]. However, the proposed model (5) and the log version model (6) are quite different, see the discussion in Section 2.1.

2.3. Existence of minimizer

For simplicity, we can define the following set:

$$\Lambda = \{(R, L) | (R, L) \in BV(\Omega) \times W^{1,2}(\Omega), \tau \leq R \leq 1, I \leq L\}. \quad (7)$$

Then the proposed model can be simplified as:

$$\min_{(R,L) \in \Lambda} E(R, L). \quad (8)$$

Theorem 1. Let $I \in L^\infty$, then the problem (8) has at least one solution in Λ .

Proof. If we let R and L be constants, the energy will be finite. Then the problem (8) is proper. Suppose $\{(R_i, L_i)\}_{i=1}^\infty \subset \Lambda$ is a minimizing sequence of the problem (8). Then there exists a constant $M > 0$ such that

$$E(R_i, L_i) \leq M. \quad (9)$$

That is,

$$\frac{1}{2} \int_{\Omega} |R_i \cdot L_i - I|^2 dx + \lambda_1 \int_{\Omega} |\nabla R_i| dx + \frac{\lambda_2}{2} \int_{\Omega} |\nabla L_i|^2 dx \leq M. \quad (10)$$

It implies

$$\int_{\Omega} |R_i \cdot L_i - I|^2 dx \leq M', \quad (11)$$

where $M' = 2M$. According to the trigonometric inequality of L^2 norm, we have

$$\int_{\Omega} |R_i \cdot L_i|^2 dx \leq C \quad (12)$$

where $C = 2 \int_{\Omega} I^2 dx + 2M'$. Combining it with

$$\tau \leq R_i \leq 1. \quad (13)$$

we can easily obtain

$$\tau \int_{\Omega} L_i^2 dx \leq \int_{\Omega} |R_i \cdot L_i|^2 dx \leq C, \quad (14)$$

which means $\int_{\Omega} L_i^2 dx$ is uniformly bounded. Then, the boundedness of $\int_{\Omega} |\nabla L_i|^2 dx$ and $\int_{\Omega} L_i^2 dx$ ensure that $\{L_i\}$ is uniformly bounded in $W^{1,2}(\Omega)$. Note that $W^{1,2}(\Omega)$ is compactly embedded in $L^2(\Omega)$, there exists a subsequence $\{L_i\}$ converging to $L_* \in W^{1,2}(\Omega)$, i.e.,

$$L_i \xrightarrow[L^2(\Omega)]{} L_* \quad \text{and} \quad L_i \rightharpoonup L_* \in W^{1,2}(\Omega). \quad (15)$$

Meanwhile, the sequence $\{R_i\}$ satisfies (13). So R_i is uniformly bounded in $L^1(\Omega)$. Combining it with the boundedness of $\lambda_1 \int_{\Omega} |\nabla R_i|$, we can get that R_i is uniformly bounded in $BV(\Omega)$. So there exists $R_* \in BV(\Omega)$ such that

$$R_i \xrightarrow[L^1(\Omega)]{} R_* \quad \text{and} \quad R_i \rightharpoonup R_* \in L^2(\Omega). \quad (16)$$

Therefore, we can get subsequence $\{(R_i, L_i)\}$ that satisfies (15) and (16). As a consequence of the lower semicontinuity for the $W^{1,2}$ norm,

$$\liminf_{i \rightarrow \infty} \left(\frac{\lambda_2}{2} \int_{\Omega} |\nabla L_i|^2 dx + \frac{\lambda_3}{2} \int_{\Omega} |L_i|^2 dx \right) \geq \frac{\lambda_2}{2} \int_{\Omega} |\nabla L_*|^2 dx + \frac{\lambda_3}{2} \int_{\Omega} |L_*|^2 dx. \quad (17)$$

Since $R_i - L_i \rightharpoonup R_* - L_*$ in $L^2(\Omega)$ and recalling the lower semicontinuity for the $L^2(\Omega)$ norm, we can obtain

$$\liminf_{i \rightarrow \infty} \frac{1}{2} \int_{\Omega} |R_i \cdot L_i - I|^2 dx \geq \frac{1}{2} \int_{\Omega} |R_* \cdot L_* - I|^2 dx. \quad (18)$$

Noting the lower semicontinuity of $BV(\Omega)$

$$\liminf_{i \rightarrow \infty} \lambda_1 \int_{\Omega} |\nabla R_i| \geq \lambda_1 \int_{\Omega} |\nabla R_*|, \quad (19)$$

we have

$$\min_{(R,L) \in \Lambda} E(R, L) = \liminf_{i \rightarrow \infty} E(R_i, L_i) \geq E(R_*, L_*). \quad (20)$$

Meanwhile, we also have $\tau \leq R_* \leq 1$ and $L_* \geq I$. This completes the proof. \square

3. Algorithm and convergence

In this section, we drive an efficient algorithm to solve the proposed model and then analyze the convergence property of the algorithm under some assumptions.

3.1. Algorithm

To solve the proposed model efficiently, we adopt the ADMM method [19] to derive the algorithm which is equivalent to the split Bregman method [20].

To facilitate an efficient use of alternating minimization, we first introduce four auxiliary variables d , u , q and v , and consider the following equivalent model:

$$\begin{aligned} & \min_{\{R,L,u,v,d,q\}} \frac{1}{2} \|RL - I\|_2^2 + \lambda_1 \|d\|_1 + \frac{\lambda_2}{2} \|q\|_2^2 + N_1(R) + N_2(L) \\ & \text{s.t.} \quad u = R, \quad d = \nabla u, \quad v = L, \quad q = \nabla v, \end{aligned} \quad (21)$$

where $N_1(R)$ and $N_2(L)$ denote the indicator functions on the constraint sets $C_1 := \{R | \tau \leq R \leq 1\}$ and $C_2 = \{L | I \leq L\}$ respectively. The augmented Lagrangian function of (21) is given by

$$\begin{aligned} \mathcal{L}_A(R, L, u, v, d, q, \Lambda_u, \Lambda_v, \Lambda_d, \Lambda_q) \\ = \frac{1}{2} \|RL - I\|_2^2 + \lambda_1 \|d\|_1 + \frac{\lambda_2}{2} \|q\|_2^2 + N_1(R) + N_2(L) \\ + \langle \Lambda_u, u - R \rangle + \langle \Lambda_v, v - L \rangle + \langle \Lambda_d, d - \nabla u \rangle + \langle \Lambda_q, q - \nabla v \rangle \\ + \frac{\sigma_1}{2} \|u - R\|_2^2 + \frac{\sigma_2}{2} \|v - L\|_2^2 + \frac{\sigma_3}{2} \|d - \nabla u\|_2^2 + \frac{\sigma_4}{2} \|q - \nabla v\|_2^2, \end{aligned} \quad (22)$$

where $\Lambda_u, \Lambda_d, \Lambda_v, \Lambda_q$ are Lagrangian multipliers, $\sigma_i \geq 0, i = 1, \dots, 4$ are penalty parameters. The ADMM algorithm for (21) is derived by minimizing \mathcal{L}_A with respect to R, L, u, v, d, q , one at a time while fixing others at their most recent values, i.e.,

$$\begin{aligned} R^{k+1} &= \arg \min_R \mathcal{L}_A(R, L^k, u^k, v^k, d^k, q^k, \Lambda_u^k, \Lambda_v^k, \Lambda_d^k, \Lambda_q^k), \\ L^{k+1} &= \arg \min_L \mathcal{L}_A(R^{k+1}, L, u^k, v^k, d^k, q^k, \Lambda_u^k, \Lambda_v^k, \Lambda_d^k, \Lambda_q^k), \\ u^{k+1} &= \arg \min_u \mathcal{L}_A(R^{k+1}, L^{k+1}, u, v^k, d^k, q^k, \Lambda_u^k, \Lambda_v^k, \Lambda_d^k, \Lambda_q^k), \\ v^{k+1} &= \arg \min_v \mathcal{L}_A(R^{k+1}, L^{k+1}, u^{k+1}, v, d^k, q^k, \Lambda_u^k, \Lambda_v^k, \Lambda_d^k, \Lambda_q^k), \\ d^{k+1} &= \arg \min_d \mathcal{L}_A(R^{k+1}, L^{k+1}, u^{k+1}, v^{k+1}, d, q^k, \Lambda_u^k, \Lambda_v^k, \Lambda_d^k, \Lambda_q^k), \\ q^{k+1} &= \arg \min_q \mathcal{L}_A(R^{k+1}, L^{k+1}, u^{k+1}, v^{k+1}, d^{k+1}, q, \Lambda_u^k, \Lambda_v^k, \Lambda_d^k, \Lambda_q^k), \end{aligned} \quad (23)$$

and then updating the Lagrangian multipliers $\Lambda_u, \Lambda_v, \Lambda_d, \Lambda_q$. It is easy to derive that the first-order optimal conditions of the subproblems in (23) are

$$0 \in L^k(R^{k+1}L^k - I) - \Lambda_u^k + \sigma_1(R^{k+1} - u^k) + \partial N_1(R^{k+1}), \quad (24a)$$

$$0 \in R^{k+1}(R^{k+1}L^{k+1} - I) - \Lambda_v^k + \sigma_2(L^{k+1} - v^k) + \partial N_2(L^{k+1}), \quad (24b)$$

$$0 = \Lambda_u^k - \nabla^T \Lambda_d^k + \sigma_1(u^{k+1} - R^{k+1}) + \sigma_3 \nabla^T(\nabla u^{k+1} - d^k), \quad (24c)$$

$$0 = \Lambda_v^k - \nabla^T \Lambda_q^k + \sigma_2(v^{k+1} - L^{k+1}) + \sigma_4 \nabla^T(\nabla v^{k+1} - q^k), \quad (24d)$$

$$0 \in \lambda_1 \partial \|d^{k+1}\|_1 + \Lambda_d^k + \sigma_3(d^{k+1} - \nabla u^{k+1}), \quad (24e)$$

$$0 = \lambda_2 q^{k+1} + \Lambda_q^k + \sigma_4(q^{k+1} - \nabla v^{k+1}). \quad (24f)$$

In the following, we solve Eq. (24a)–(24f) one by one. Since the constraint set C_1 of R in N_1 is convex, from (24a) it is direct to derive the updating formula of R as

$$R^{k+1} = \mathcal{P}_1 \left(\frac{L^k I + \Lambda_u^k + \sigma_1 u^k}{(L^k)^2 + \sigma_1} \right), \quad (25)$$

where \mathcal{P}_1 denotes the projection on the convex set C_1 which is defined as $(\mathcal{P}_1(z))_{ij} = \min(\max(z_{ij}, \tau), 1)$. Similarly, since the constraint set C_2 of L in N_2 is also convex, from (24b) we can derive the updating formula of L as

$$L^{k+1} = \mathcal{P}_2 \left(\frac{R^{k+1} I + \Lambda_v^k + \sigma_2 v^k}{(R^{k+1})^2 + \sigma_2} \right), \quad (26)$$

where \mathcal{P}_2 denotes the projection on the convex set C_2 which is defined as $(\mathcal{P}_2(z))_{ij} = \max(z_{ij}, I_{ij})$. From (24c) and (24d), by direct computation, we get the updating formulas of u and v as

$$u^{k+1} = (\sigma_1 + \sigma_3 \nabla^T \nabla)^{-1} (\nabla^T \Lambda_d^k - \Lambda_u^k + \sigma_1 R^{k+1} + \sigma_3 \nabla^T d^k), \quad (27)$$

$$v^{k+1} = (\sigma_2 + \sigma_4 \nabla^T \nabla)^{-1} (\nabla^T \Lambda_q^k - \Lambda_v^k + \sigma_2 L^{k+1} + \sigma_4 \nabla^T q^k). \quad (28)$$

Note that the update of u^{k+1} and v^{k+1} can be implemented by fast Fourier transform (FFT) and inverse fast Fourier transform (IFFT) very efficiently. From (24e), by using the definition of sub-gradient of L_1 norm, we can derive that the updating formula of d is given by soft shrinkage:

$$d^{k+1} = \mathcal{S}\left(\nabla u^{k+1} - \frac{\Lambda_d^k}{\sigma_3}, \frac{\lambda_1}{\sigma_3}\right). \quad (29)$$

where \mathcal{S} denotes the soft shrinkage operator defined as

$$(\mathcal{S}(s, c))_{ij} := \frac{s_{ij}}{|s_{i,j}|} * \max(|s_{i,j}| - c, 0).$$

Finally, from (24f), it is easy to derive the updating formula for q as

$$q^{k+1} = \frac{\sigma_4 \nabla v^{k+1} - \Lambda_q^k}{\sigma_4 + \lambda_2}. \quad (30)$$

According to the standard ADMM algorithm, the updating formulas for the Lagrangian multipliers Λ_u , Λ_v , Λ_d , Λ_q are given by

$$\Lambda_u^{k+1} = \Lambda_u^k + \sigma_1(u^{k+1} - R^{k+1}), \quad (31)$$

$$\Lambda_v^{k+1} = \Lambda_v^k + \sigma_2(v^{k+1} - L^{k+1}), \quad (32)$$

$$\Lambda_d^{k+1} = \Lambda_d^k + \sigma_3(d^{k+1} - \nabla u^{k+1}), \quad (33)$$

$$\Lambda_q^{k+1} = \Lambda_q^k + \sigma_4(q^{k+1} - \nabla v^{k+1}). \quad (34)$$

Finally, the proposed numerical algorithm for solving model (5) can be summarised in [Algorithm 1](#). The stopping criterion is that the following relative errors between the successive iterations satisfy

$$\epsilon_R = ||R^k - R^{k-1}|| / ||R^{k-1}|| < tol,$$

or

$$\epsilon_L = ||L^k - L^{k-1}|| / ||L^{k-1}|| < tol.$$

3.2. Convergence

Note that problem (21) is nonconvex and the global convergence is difficult to analyze. Inspired by the convergence analysis of the ADMM algorithm for matrix completion with nonnegative factors [21], We provide a convergence property of the proposed [Algorithm 1](#) that holds under some assumptions.

Algorithm 1 The proposed Retinex algorithm.

- Input I , $maxiter > 0$, and $tol > 0$. Set $\lambda_1 > 0$, $\lambda_2 > 0$, $\sigma_1 > 0$, $\sigma_2 > 0$, $\sigma_3 > 0$, $\sigma_4 > 0$.
 - Initialize $L^0 = I$, $v^0 = I$, $q^0 = \nabla I$ and R^0 , u^0 , d^0 , Λ_u^0 , Λ_v^0 , Λ_d^0 , Λ_q^0 are zero matrices with appropriate sizes.
 - **for** $k = 1, \dots, maxiter$ **do**
 - Update R^k by (25);
 - Update L^k by (26);
 - Update u^k by (27);
 - Update v^k by (28);
 - Update d^k by (29);
 - Update q^k by (30);
 - Update Λ_u^k by (31);
 - Update Λ_v^k by (32);
 - Update Λ_d^k by (33);
 - Update Λ_q^k by (34);
 - if** a stopping criterion is reached
 - then** exit and output (R^k, L^k)
 - end if** - **end for**
-

To simplify notation, we define $X = (R, L, u, v, d, q)$ and $Y = (\Lambda_u, \Lambda_v, \Lambda_d, \Lambda_q)$, and write $\mathcal{L}_A(R)$ to represent the augmented Lagrangian function with respect to X by fixing others at their most recent values. A point (X, Y) is a KKT point of the problem (21) if there exist $\Lambda_u, \Lambda_v, \Lambda_d$, and Λ_q such that

$$\begin{aligned} 0 &\in RL^2 - LI - \Lambda_u + \partial N_1(R), \\ 0 &\in LR^2 - RI - \Lambda_v + \partial N_2(L), \\ 0 &= \Lambda_u - \nabla^T \Lambda_d, \\ 0 &= \Lambda_v - \nabla^T \Lambda_q, \\ 0 &\in \lambda_1 \partial \|d\|_1 + \Lambda_d, \\ 0 &= \lambda_2 q + \Lambda_q, \\ u &= R, \\ v &= L, \\ d &= \nabla u, \\ q &= \nabla v. \end{aligned} \tag{35}$$

In the following, we assume that $\{(X^k, Y^k)\}$ is a sequence generated by the proposed Algorithm 1. We give the convergence analysis of the sequence.

Lemma 1. If the multiplier sequence Y^k is bounded and satisfies

$$\sum_{k=0}^{\infty} (\|\Lambda_u^{k+1} - \Lambda_u^k\|_2^2 + \|\Lambda_v^{k+1} - \Lambda_v^k\|_2^2 + \|\Lambda_d^{k+1} - \Lambda_d^k\|_2^2 + \|\Lambda_q^{k+1} - \Lambda_q^k\|_2^2) < \infty, \tag{36}$$

then $X^{k+1} - X^k \rightarrow 0, Y^{k+1} - Y^k \rightarrow 0$.

See the proof of Lemma 1 in the appendix.

Theorem 2. If the multiplier sequence Y^k is bounded and satisfies the inequality (36), then any accumulation point of $\{(X^k, Y^k)\}$ satisfies the KKT condition for problem (21). Consequently, any accumulation point of $\{(R^k, L^k)\}$ satisfies the KKT condition for problem (5).

Proof. By Lemma 1, we have that $X^{k+1} - X^k \rightarrow 0, Y^{k+1} - Y^k \rightarrow 0$. According to the updating formulas of Algorithm 1 in (25)–(34), we rewrite them in the following equivalent formulation:

$$R^{k+1} - R^k = \mathcal{P}_1 \left(\frac{L^k I + \Lambda_u^k + \sigma_1 u^k}{(L^k)^2 + \sigma_1} \right) - R^k, \tag{37a}$$

$$L^{k+1} - L^k = \mathcal{P}_2 \left(\frac{R^{k+1} I + \Lambda_v^k + \sigma_2 v^k}{(R^{k+1})^2 + \sigma_2} \right) - L^k, \tag{37b}$$

$$(\sigma_1 + \sigma_3 \nabla^T \nabla)(u^{k+1} - u^k) = \Phi_1, \tag{37c}$$

$$(\sigma_2 + \sigma_4 \nabla^T \nabla)(v^{k+1} - v^k) = \Phi_2, \tag{37d}$$

$$d^{k+1} - d^k = \mathcal{S} \left(\nabla u^{k+1} - \frac{\Lambda_d^k}{\sigma_3}, \frac{\lambda_1}{\sigma_3} \right) - d^k, \tag{37e}$$

$$q^{k+1} - q^k = \frac{\sigma_4 \nabla v^{k+1} - \Lambda_q^k}{\sigma_4 + \lambda_2} - q^k, \tag{37f}$$

$$\Lambda_u^{k+1} - \Lambda_u^k = \sigma_1(u^{k+1} - R^{k+1}), \tag{37g}$$

$$\Lambda_v^{k+1} - \Lambda_v^k = \sigma_2(v^{k+1} - L^{k+1}), \tag{37h}$$

$$\Lambda_d^{k+1} - \Lambda_d^k = \sigma_3(d^{k+1} - \nabla u^{k+1}), \tag{37i}$$

$$\Lambda_q^{k+1} - \Lambda_q^k = \sigma_4(q^{k+1} - \nabla v^{k+1}). \quad (37j)$$

where

$$\Phi_1 := \nabla^T \Lambda_d^k - \Lambda_u^k + \sigma_1(R^{k+1} - u^k) + \sigma_3 \nabla^T(d^k - \nabla u^k),$$

$$\Phi_2 := \nabla^T \Lambda_q^k - \Lambda_v^k + \sigma_2(L^{k+1} - v^k) + \sigma_4 \nabla^T(q^k - \nabla v^k).$$

Letting $k \rightarrow \infty$ and using $X^{k+1} - X^k \rightarrow 0$ and $Y^{k+1} - Y^k \rightarrow 0$, we get both the left-hand side and the right-hand side of the above equations all goes to zero such that

$$0 \leftarrow \mathcal{P}_1 \left(\frac{L^k I + \Lambda_u^k + \sigma_1 u^k}{(L^k)^2 + \sigma_1} \right) - R^k, \quad (38a)$$

$$0 \leftarrow \mathcal{P}_2 \left(\frac{R^{k+1} I + \Lambda_v^k + \sigma_2 v^k}{(R^{k+1})^2 + \sigma_2} \right) - L^k, \quad (38b)$$

$$0 \leftarrow \nabla^T \Lambda_d^k - \Lambda_u^k + \sigma_1(R^{k+1} - u^k) + \sigma_3 \nabla^T(d^k - \nabla u^k), \quad (38c)$$

$$0 \leftarrow \nabla^T \Lambda_q^k - \Lambda_v^k + \sigma_2(L^{k+1} - v^k) + \sigma_4 \nabla^T(q^k - \nabla v^k), \quad (38d)$$

$$0 \leftarrow \mathcal{S} \left(\nabla u^{k+1} - \frac{\Lambda_d^k}{\sigma_3}, \frac{\lambda_1}{\sigma_3} \right) - d^k, \quad (38e)$$

$$0 \leftarrow \frac{\sigma_4(\nabla v^{k+1} - q^k) - \Lambda_q^k - \lambda_2 q^k}{\sigma_4 + \lambda_2}, \quad (38f)$$

$$0 \leftarrow u^k - R^k, \quad (38g)$$

$$0 \leftarrow v^k - L^k, \quad (38h)$$

$$0 \leftarrow d^k - \nabla u^k, \quad (38i)$$

$$0 \leftarrow q^k - \nabla v^k. \quad (38j)$$

It is easy to derive that (38a), (38b) and (38e) are equivalent to

$$0 \leftarrow L^k(R^k L^k - I) - \Lambda_u^k + \sigma_1(R^k - u^k) + \partial N_1(R^k), \quad (39a)$$

$$0 \leftarrow R^{k+1}(R^{k+1} L^k - I) - \Lambda_v^k + \sigma_2(L^k - v^k) + \partial N_2(L^k), \quad (39b)$$

$$0 \leftarrow \lambda_1 \partial \|d^k\|_1 + \Lambda_d^k + \sigma_3(d^k - \nabla u^{k+1}). \quad (39c)$$

Note that in (38) and (39) the terms involving $R^k - u^k$, $R^{k+1} - u^k$, $L^k - v^k$, $L^{k+1} - v^k$, $d^k - \nabla u^k$, $d^k - \nabla u^{k+1}$, and $q^k - \nabla v^k$ can be eliminated by using (38g)-(38j) when letting $k \rightarrow \infty$. For any limit point \hat{X} of sequence $\{X^k\}$, there exists subsequence $\{X^{n_k}\}$ converging to \hat{X} . The boundedness of $\{Y^k\}$ implies the existence of a subsequence $\{Y^{n_{k_j}}\}$ converging to some point \hat{Y} . Hence, (\hat{X}, \hat{Y}) is a limit point of the sequence $\{(X^k, Y^k)\}$. Letting $k \rightarrow \infty$ in (38) and (39), it is straightforward to verify that (\hat{X}, \hat{Y}) is a KKT point of the problem (21). Thus (\hat{R}, \hat{L}) is a KKT point of the original Retinex problem (5) which follows directly from the equivalence between the two problems (5) and (21). This completes the proof. \square

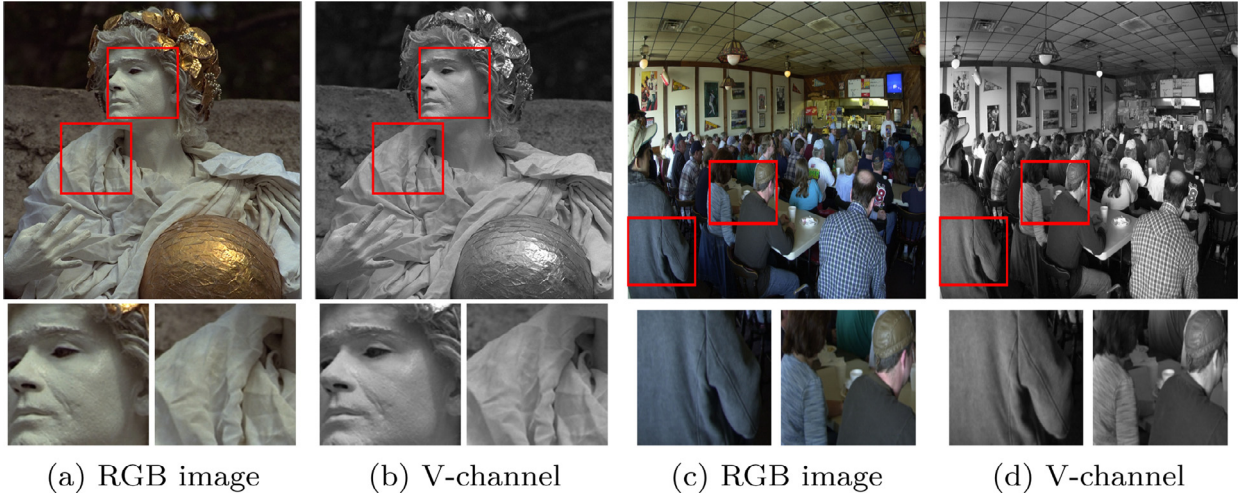


Fig. 2. RGB images and the corresponding V-channels.

4. Numerical results

We perform all the experiments on a PC with Intel Core i7 CPU 6800k, 64GB RAM. The programming language for all methods is MATLAB. We compare our model with three state-of-art methods including the methods in [13,17,18]. To be fair, we use the codes from the author with default parameters. In our experiments, we empirically set the parameters $\lambda_1 = 0.01$, $\lambda_2 = 0.1$, $\sigma_1 = 5$, $\sigma_2 = 5$, $\sigma_3 = 0.02$ and $\sigma_4 = 5$, respectively. Besides, we set the stop parameters as $\epsilon = 10^{-3}$ and the lower bounded of reflectance as $\tau = 10^{-4}$. Following the previous methods [13], for color images, we first transform the color images into the HSV space and then apply our Retinex method to decompose the V-channel as reflectance and illumination.

4.1. Reflectance and illumination estimation

We first show the results of different methods for reflectance and illumination estimation in Figs. 2 and 3. Fig. 2 shows the original RGB images and their V-channels. Note that the V-channel is the input for the proposed Algorithm 1 and the other three compared methods. From Fig. 3, it is obvious that the illumination estimated by our method is smoother and contains less information about the input image than others. The estimated reflectance from [13] (see Fig. 3(e) and (m)) is obviously fuzzy and loses lots of details. Though the reflectance estimated from [17] (see Fig. 3(f) and (n)) seems much better, it is still fuzzy and losing some details. In Fig. 3(f), we can see that the textures on the face and the clothes on the shoulder disappear to some extent. The same phenomenon also appears in Fig. 3(n). It is the side effect of the log-transform as discussed in Section 2.1. The estimated L from [18] contains many image details. Meanwhile, as can be seen from Fig. 3(g) and (o), the estimated reflectance images look dark. In this sense, their decomposition results are not satisfactory. While in our estimated reflectance, the textures and details are preserved well. In a whole, our reflectance images preserve details effectively and the illumination images are smoother than the other methods.

As we know, the purpose of Retinex theory is to decompose the reflectance and the illumination from an observed image. In this experiment, we will evaluate the image recovered from the estimated reflectance and the illumination of different models by computing difference between the recovered result and the input V-channel image as follows:

$$D = L \cdot R - S_0, \quad (40)$$

where S_0 is the V-channel of the input RGB image. Mean-Square Error (MSE) is used to measure the difference quantitatively. Fig. 4 shows the results. Fig. 4(b) and (g), (c) and (h), (d) and (i), (e) and (j) is the difference images from methods in [13,17,18] and the proposed method, respectively. As can be seen both from the difference images and the MSE values, the proposed method has the smallest MSE measure. That means, the proposed method decomposes the input images into reflectance and illumination more accurately than others. Hence more details are kept in both the reflectance and the illumination.

4.2. Image enhancement

For image enhancement, Gamma correction is widely used to enhance the illumination channel as follows:

$$L' = W \left(\frac{L}{W} \right)^{\frac{1}{\gamma}}, \quad (41)$$

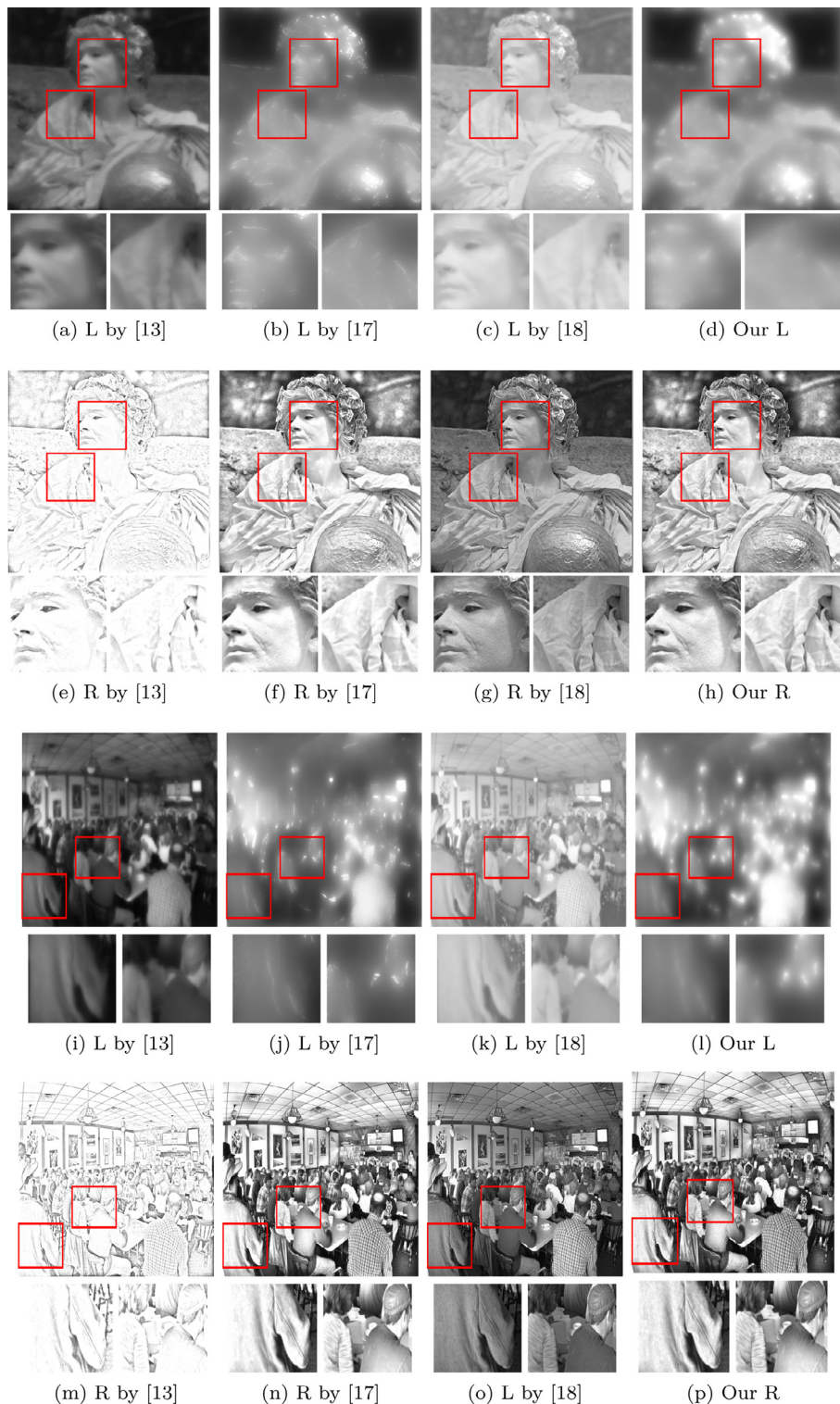


Fig. 3. Comparison of the estimated illumination and reflectance for V-channels.

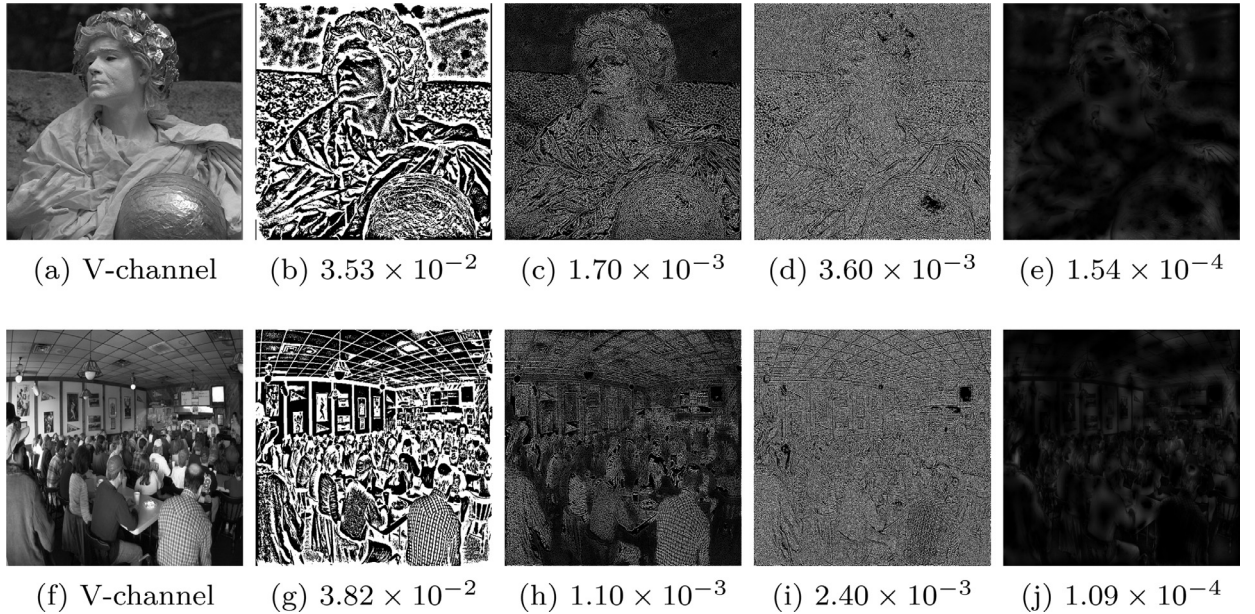


Fig. 4. Decomposition difference between different models. The number below each image is the MSE value. The images from the second column to the last column are difference images by the methods in [13,17,18] and the proposed method, respectively.

where W is equal to 255 for an 8-bit image. In [13], their model estimated the reflectance and illumination simultaneously, but the estimated reflectance is obviously fuzzy. Hence they chose to estimate the reflectance by

$$R' = \frac{I}{L} \quad (42)$$

and then computed the enhanced images using the following formula:

$$I_{\text{enhanced}} = R' \cdot L'. \quad (43)$$

In [17], the reflectance component seems good and the enhanced results are given by

$$I_{\text{enhanced}} = R \cdot L'. \quad (44)$$

In [18], different from the methods mentioned above, the authors do the decomposition on the three channels of the input RGB image simultaneously and obtain the low-light enhancement result only using the estimated R :

$$I_{\text{enhanced}} = \left(\frac{S}{g_y} \right)^\rho \cdot R, \quad (45)$$

where S and g_y respectively represent the input RGB image and its luminance. In our method, we prefer to performing Gamma correction on both the estimated illumination and the estimated reflectance

$$R' = R^{\frac{1}{\gamma_1}}, L' = W \left(\frac{L}{W} \right)^{\frac{1}{\gamma_2}}, \quad (46)$$

and then obtain the final enhanced result:

$$I_{\text{enhanced}} = R' \cdot L'. \quad (47)$$

Empirically, we set γ_1 and γ_2 as 2.3 and 2.8, respectively.

Fig. 5 demonstrates some examples of enhanced results. As can be seen, because of the side effect of the log-transform, the enhanced results from [13] are obviously over-lighted and fuzzy, and some details are lost. The visual effects of [17] and our model are similar, which seems more natural than others. Reflectance images from [18] are darker which implies that estimated reflectance images still include the illumination component.

Since there is no ground truth for the enhanced images, we use a blind image quality assessment called natural image quality evaluator (NIQE) [22] to evaluate the results. The lower NIQE value is, the better image quality the result has. Table 1 shows that the proposed model has the lowest NIQE value among all for each image. Averagely, our model is the best, [17] is the second best, and [18] is the worst among all.

Moreover, we perform the test on three widely used datasets including the non-uniform illumination image dataset [23], the Berkeley Segmentation dataset [24], the Pku-EAQA dataset [25]. As shown in Table 2, the proposed model has the lowest NIQE value on each dataset which indicates that the proposed model achieves the best performance among all.

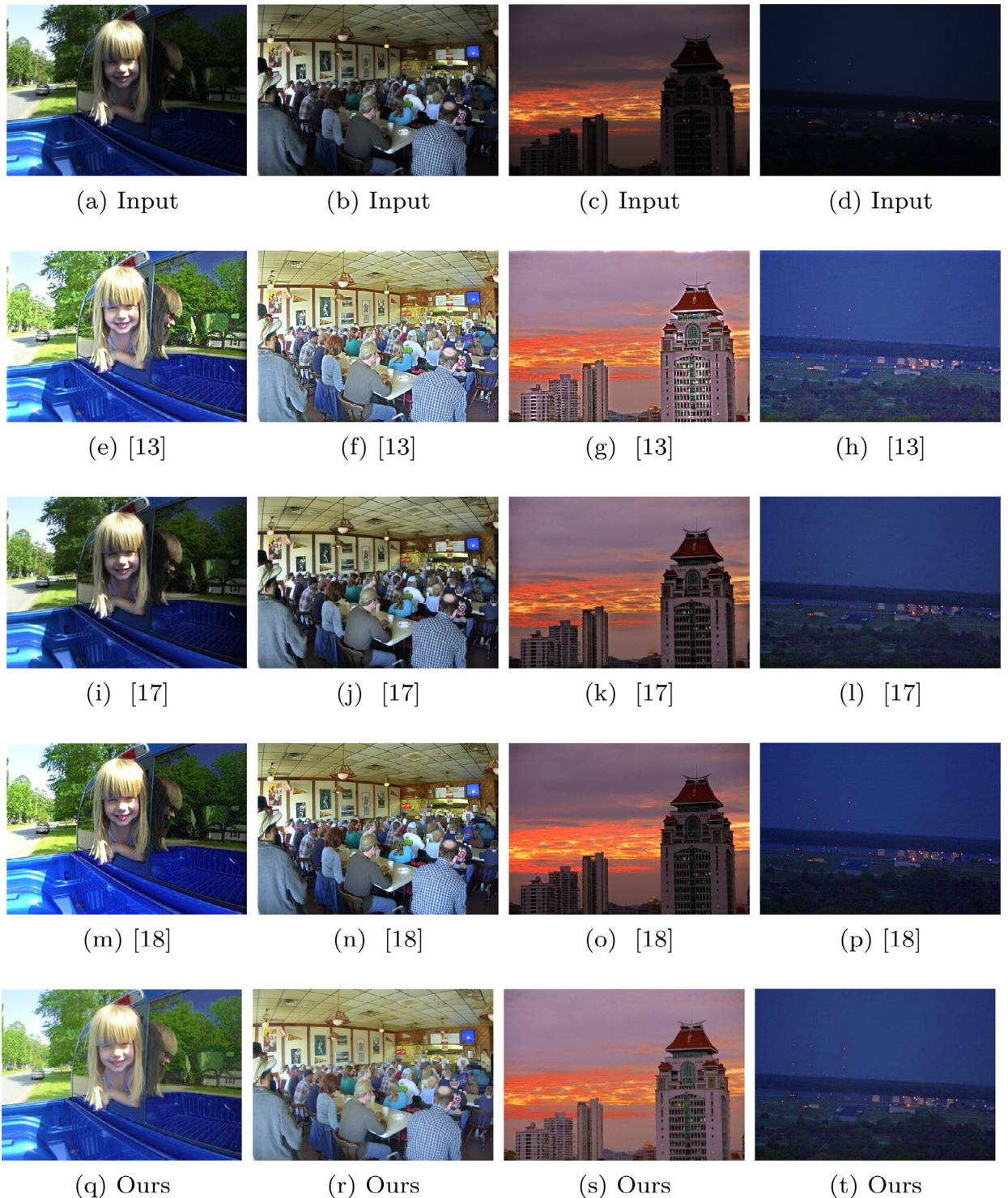


Fig. 5. Comparison of the enhanced results of four color images by different methods.

Table 1
Average NIQE values of Fig. 5.

Rows	Inputs	[13]	[17]	[18]	Ours
1st col	2.98	3.09	2.79	3.21	2.62
2nd col	2.52	2.17	2.38	3.44	2.15
3rd col	3.74	3.20	3.65	4.35	3.10
4th col	6.19	4.37	3.98	4.95	3.92
Average	3.86	3.21	3.20	3.74	2.95

Table 2
Average NIQE values on four datasets.

Datasets	Inputs	[13]	[17]	[18]	Ours
Non-uniform	3.66	3.72	3.40	4.19	3.40
Berkeley Seg	3.30	3.28	3.24	4.80	3.17
Pku-EAQA	4.40	4.63	4.20	6.25	4.17

4.3. Noise sensitivity

As we know, when applying Gamma correction, the noise in the dark areas will be enlarged. How to suppress it is an interesting task. In this experiment, the slight additive white Gaussian noise n with $\sigma = 5$ is added into two dark images:

$$I = R \cdot L + n. \quad (48)$$

In the proposed model, the fidelity term is

$$\|I - R \cdot L\|_2^2 = \|n\|_2^2. \quad (49)$$

While in the log-transform based methods such as [13] and [17], the fidelity term is

$$\|I - L - r\|_2^2 = \|\log\left(1 + \frac{n}{R \cdot L}\right)\|_2^2. \quad (50)$$

In [18], the fidelity term is

$$\|I - R \cdot L\|_2^2 + \|L - L_0\|_2^2 = \|n\|_2^2 + \|L - L_0\|_2^2, \quad (51)$$

where L_0 is estimated by applying the Gauss-low filter to the input image. The estimation of L_0 is far from accurate such that the fidelity is hard to control. Comparing the three fidelity terms, we find that the proposed fidelity term (49) is more reasonable than others when n is additive Gaussian noise.

The numerical results are shown in Fig. 6 for two test images. It can be seen that all the methods are somewhat sensitive to noise. Visually, we find that the results of our method are relatively cleaner than others. For quantitative assessment, we report the signal-to-noise ratio (SNR) of each result. The SNR values of our method are the highest among all, which is consistent with the observation.

4.4. Impact of parameters and initial value

The default values of λ_1 and λ_2 in the proposed model are set as 0.01 and 0.1. In order to illustrate the impact of the parameters to the estimated results, we change one of them while keeping another unchanged. The resulted reflectance and illumination images are displayed in Fig. 7. In the first two rows, we set λ_1 as 0.01. It is obvious that as λ_2 increases from 0.01 to 1, the illumination image in the first row becomes smoother and smoother, while the reflectance in the second row contains more and more details. In the last two rows, we fix λ_2 as 0.1. As λ_1 increases from 0.01 to 1, we find that the reflectance and illumination images are almost the same. This means that the proposed method is more sensitive to λ_2 than λ_1 .

In the proposed algorithm, actually, only the initial value of L^0 is required. Fig. 8 shows the iteration results from the different initial value of L^0 . We show the intermediate results of reflectance when iteration is 1, 5 and 180, respectively. We find that after five iterations, the results become similar. After 180 iterations, the results seem very similar. The experiment implies that the proposed algorithm is robust to initialization.

4.5. Convergence rate and computational time

Fig. 9 shows the convergence rate of the proposed model between error and iteration numbers (test image is Fig. 2(b)). As can be seen, the convergence rate curve is pretty smooth and the convergence rate is relatively fast. It can be attributed to the ADMM algorithm which split the original problem (5) into six sub-problems that have closed-form solutions. We also

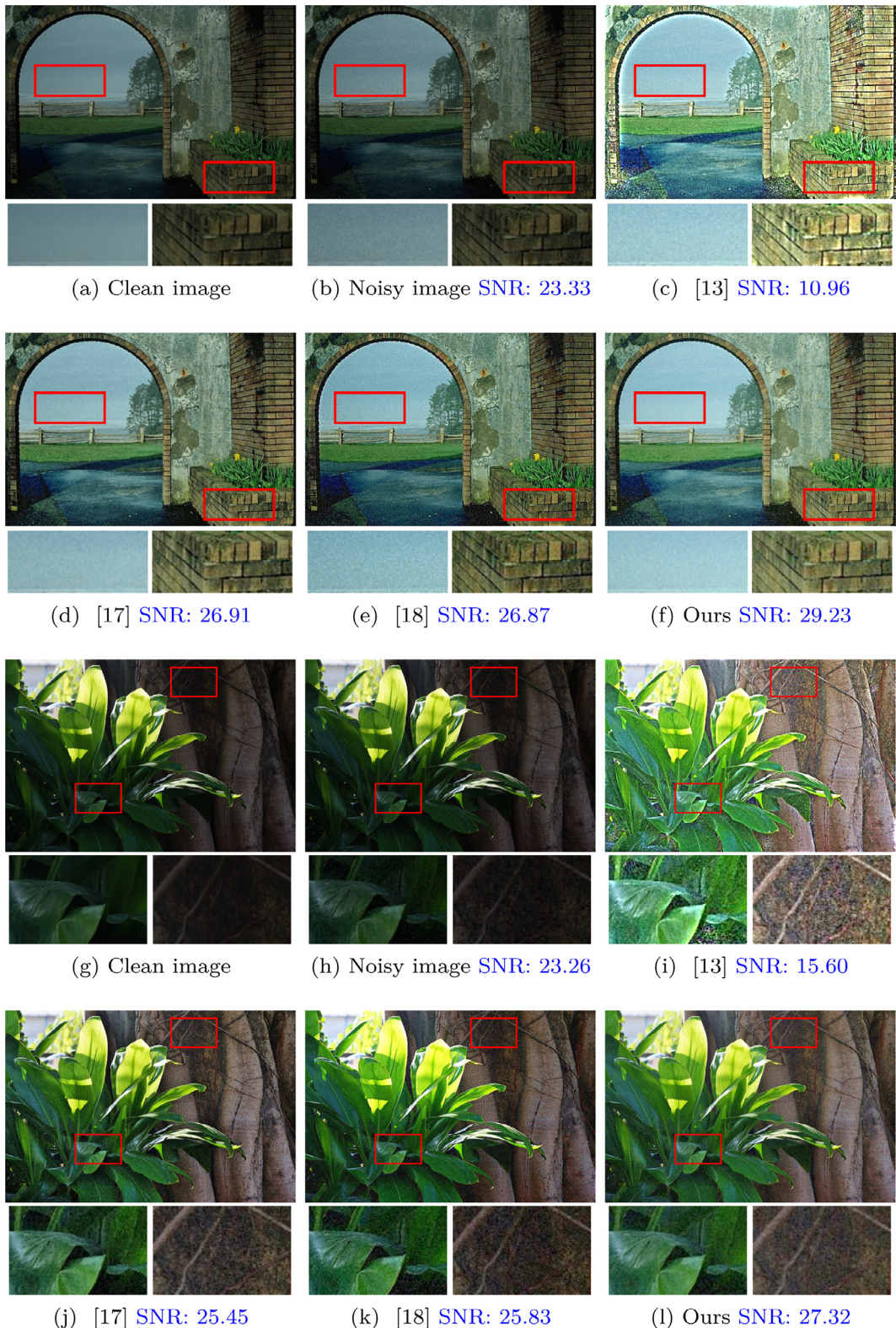


Fig. 6. Comparison of noise suppression by different models. The magnified areas are corresponding to the parts signed by the red rectangles. The number under each image is signal-to-noise ratio value.

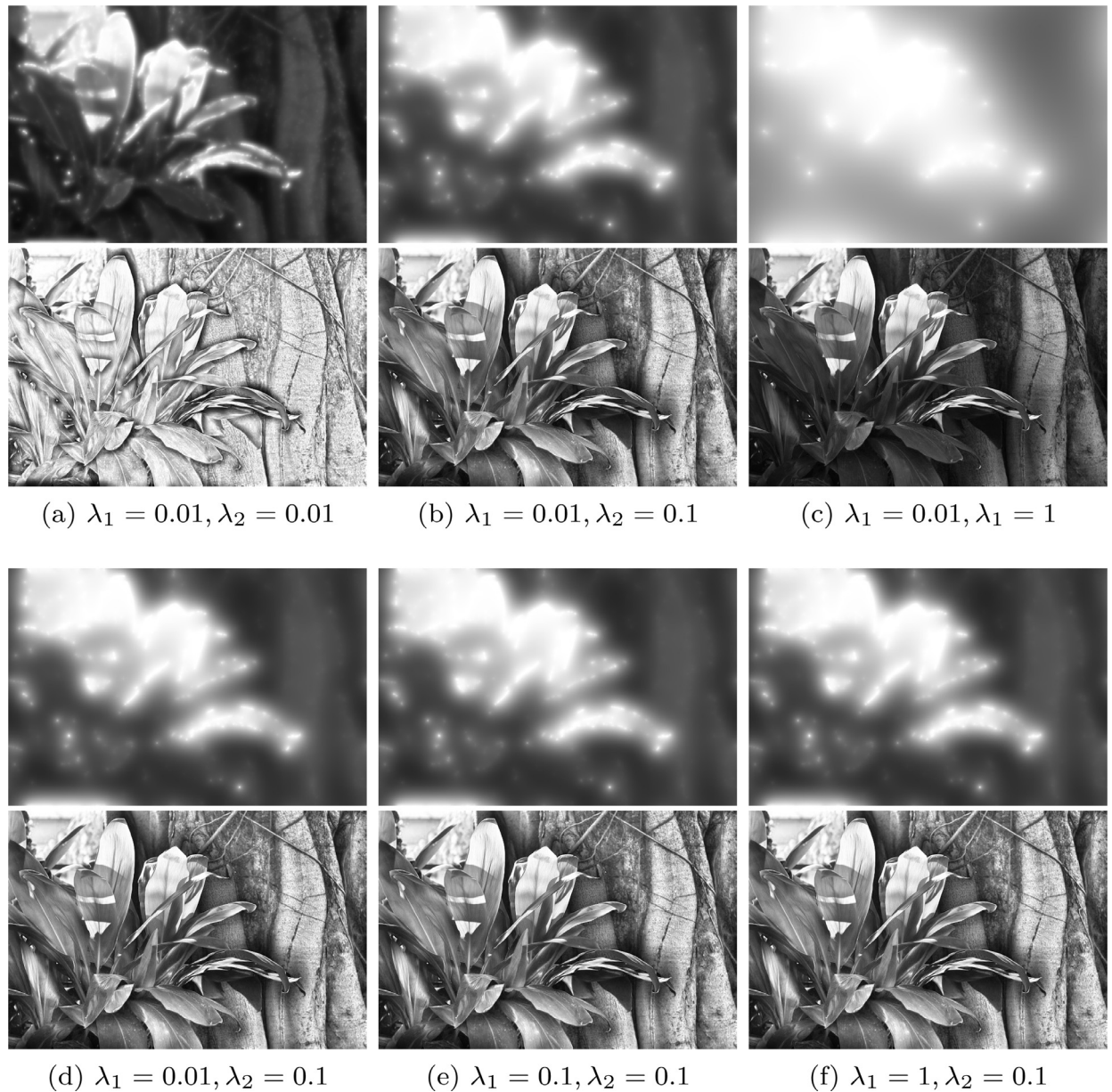


Fig. 7. Examples of the impact of λ_1 and λ_2 . The number under each image are λ_1, λ_2 respectively.

Table 3
Average computational time (sec) of different methods when applied to images with different size.

Methods	321×481	1400×2100
[13]	0.66	8.20
[17]	8.18	341.28
[18]	6.98	104.63
Our model	4.15	71.72

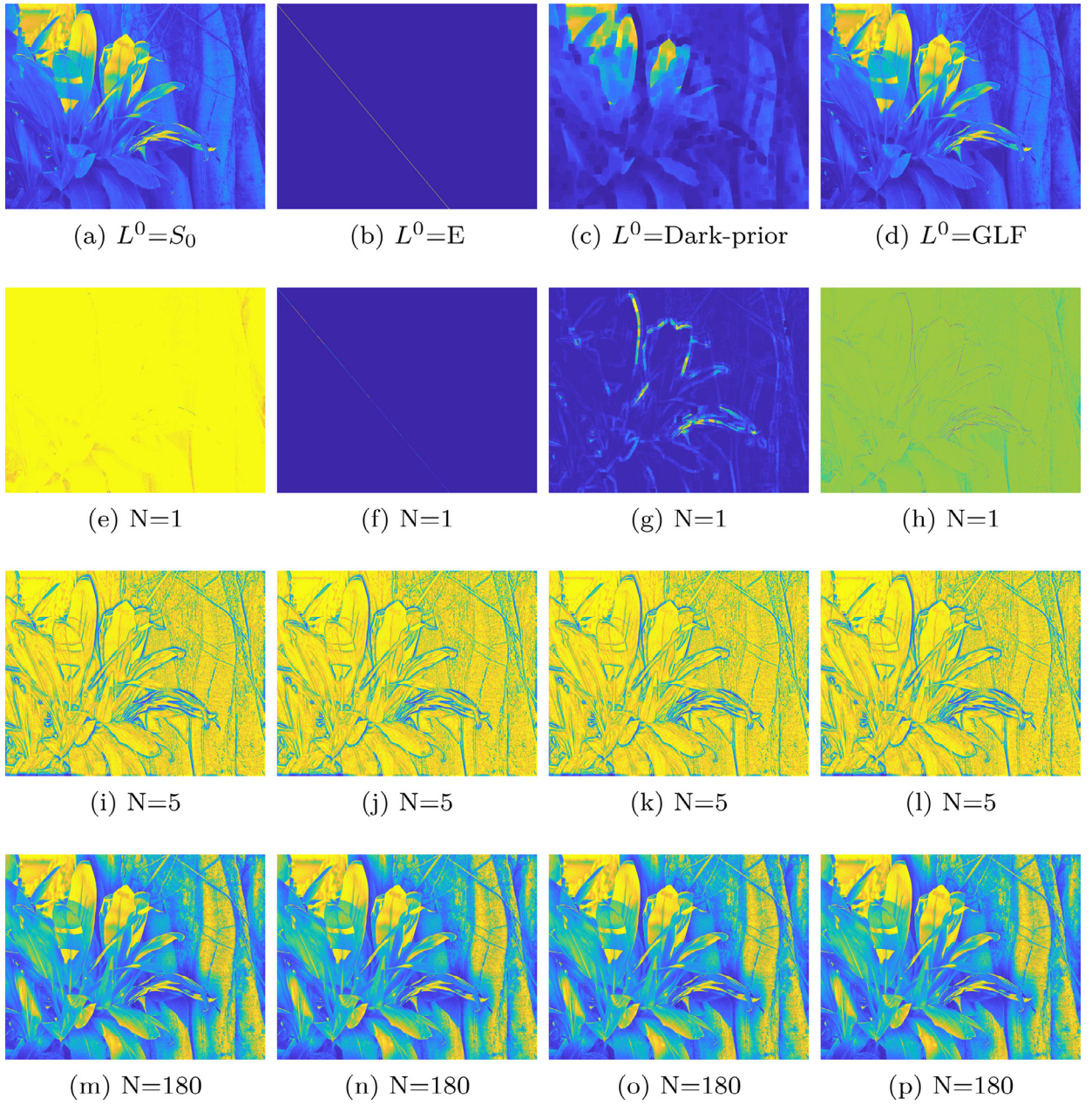


Fig. 8. Examples of the impact of different initial values of L^0 . S^0 is the V-channel of the input RGB image, E is the identity matrix, Dark-prior is the image after the dark-prior operation from [26], GLF denotes the result by applying the Gauss-low filter on S_0 , N is the iteration number.

test the computational time of the proposed model on images with the different size which are chosen from [24] and Google image searching respectively. Table 3 shows the comparison result. Among all, [13] is the fastest since only two iterations are performed as suggested by the author. The other methods are stopped with some error criterion and more iterations are required. We can conclude that the proposed model has a good trade-off between computing speed and enhanced image quality.

5. Limitations and discussions

In this paper, we propose a detail preserving variational model for image Retinex. Different from the log-transform based models, the proposed model performs the decomposition directly in the image domain. Compared with the log-transform based methods, the advantage of the proposed method is that the details can be preserved well in the reflectance component. However, there are some limitations. Firstly, the assumption that the illumination is smooth is not satisfied in some

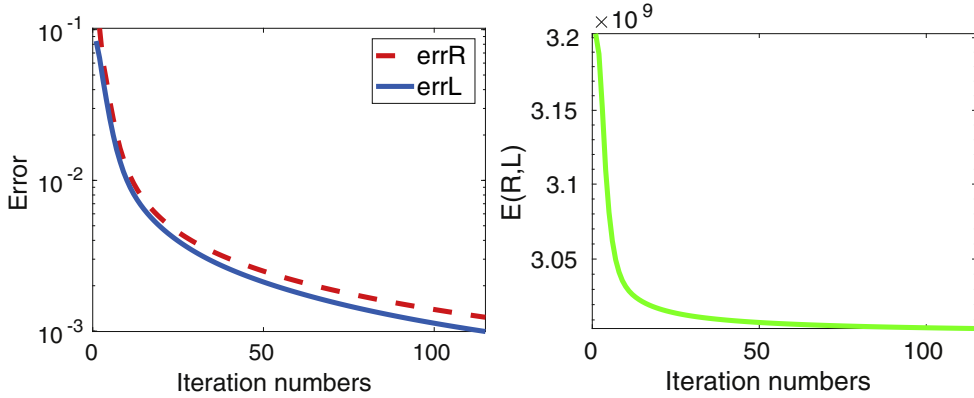


Fig. 9. Left image: the relationship between error and iteration numbers. Right image: the relationship between energy function $E(R, L)$ and iteration numbers.

images with shadows. In this case, the illumination is better to be modeled as piecewise smooth. Secondly, similar to other compared models, the noise suppression ability of the proposed model is limited. Thirdly, the Gamma correction step is required for all of the compared methods when applied to image enhancement. Similar as the other compared methods, our method is sensitive to the Gamma correction parameters. In Fig. 10(a), we plot the surface of NIQE when the gamma correction parameters are varying. The surface is not smooth and the amplitude is large. In Fig. 10(b)–(d), three enhanced results with different gamma are displayed, which are very different. This demonstrates that the enhanced result of our proposed method is sensitive to the Gamma correction parameters.

In the future work, we will study new methods in order to overcome the above limitations which including using the assumption that the illumination is piecewise smooth, adding noise suppression terms in the decomposition model, and designing Gamma correction free image enhancement algorithm.

Acknowledgments

The authors would like to thank W. Wang and X. Fu for sharing the codes of [13] and [17], respectively. The authors also thank Wang et al., Martin et al. and Chen et al. for offering the non-uniform illumination image dataset [23], the Berkeley Segmentation dataset [24] and the Pku-EAQA dataset [25], respectively.

Appendix. Proof of Lemma 1

Proof. By the definition of $\mathcal{L}_A(X^k, Y^k)$ and the boundedness of Y^k , we obtain that $\mathcal{L}_A(X^k, Y^k)$ is bounded below. Furthermore, it is straightforward to verify that the augmented Lagrangian function \mathcal{L}_A is strongly convex with respect to each variable of R , L , u , v , d , and q . Hence, for variable R , it holds that

$$\mathcal{L}_A(R + \Delta R) - \mathcal{L}_A(R) \geq \partial_R \mathcal{L}_A(R) \Delta R + \sigma_1 \|\Delta R\|_2^2. \quad (52)$$

In addition, R^{k+1} is a minimizer of $\mathcal{L}_A(R)$ at the k th iteration implies

$$\partial_R \mathcal{L}_A(R^{k+1}) \Delta R \geq 0. \quad (53)$$

Hence, we have

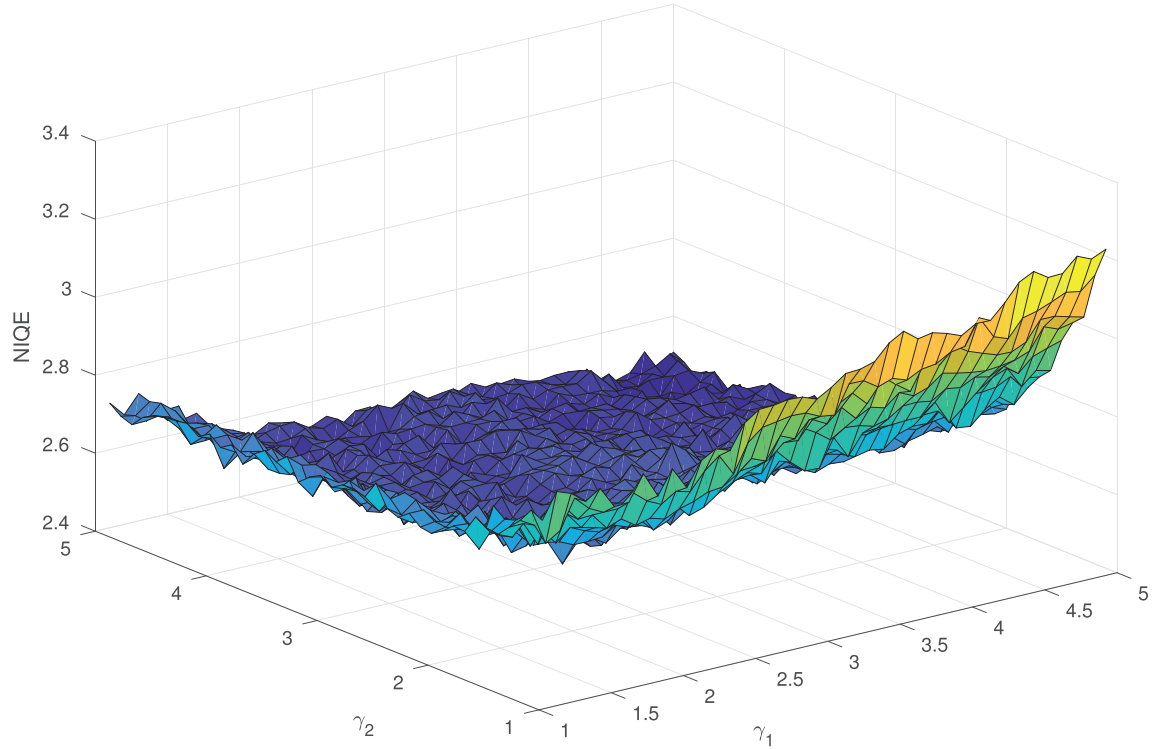
$$\mathcal{L}_A(R^k) - \mathcal{L}_A(R^{k+1}) \geq \sigma_1 \|R^k - R^{k+1}\|_2^2. \quad (54)$$

By similar arguments, we get

$$\begin{aligned} \mathcal{L}_A(L^k) - \mathcal{L}_A(L^{k+1}) &\geq \sigma_2 \|L^k - L^{k+1}\|_2^2, \\ \mathcal{L}_A(u^k) - \mathcal{L}_A(u^{k+1}) &\geq \sigma_1 \|u^k - u^{k+1}\|_2^2, \\ \mathcal{L}_A(v^k) - \mathcal{L}_A(v^{k+1}) &\geq \sigma_2 \|v^k - v^{k+1}\|_2^2, \\ \mathcal{L}_A(d^k) - \mathcal{L}_A(d^{k+1}) &\geq \sigma_3 \|d^k - d^{k+1}\|_2^2, \\ \mathcal{L}_A(q^k) - \mathcal{L}_A(q^{k+1}) &\geq \sigma_4 \|q^k - q^{k+1}\|_2^2. \end{aligned} \quad (55)$$

Let $c = \min\{\sigma_1, \sigma_2, \sigma_3, \sigma_4\}$. Then by (54) and (55), we have

$$\mathcal{L}_A(X^k, Y^k) - \mathcal{L}_A(X^{k+1}, Y^{k+1}) = \mathcal{L}_A(X^k, Y^k) - \mathcal{L}_A(X^{k+1}, Y^k) + \mathcal{L}_A(X^{k+1}, Y^k) - \mathcal{L}_A(X^{k+1}, Y^{k+1})$$



(a) NIQE surface of different gamma correction parameters (γ_1, γ_2) .

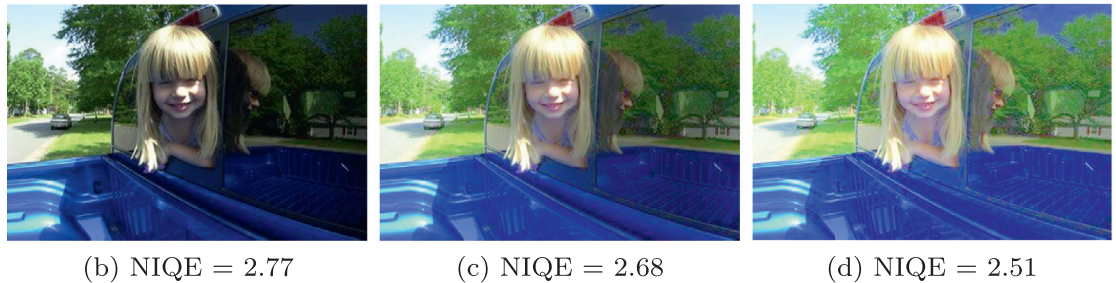


Fig. 10. Impact of gamma correction parameters γ_1 and γ_2 . The test image is Fig. 5(a). (a) is the surface of NIQE as function of γ_1 and γ_2 ; (b) the enhanced image with $\gamma_1 = 1.2$ and $\gamma_2 = 1.5$; (c) the enhanced image with $\gamma_1 = 3$ and $\gamma_2 = 2$; (d) the enhanced image with $\gamma_1 = 5$ and $\gamma_2 = 5$.

$$\geq c \|X^k - X^{k+1}\|_2^2 - \frac{1}{c} \|Y^k - Y^{k+1}\|_2^2 \quad (56)$$

Taking summation of the above inequality and recalling \mathcal{L}_A is bounded below, we get

$$\sum_{k=0}^{\infty} c \|X^k - X^{k+1}\|_2^2 - \sum_{k=0}^{\infty} \frac{1}{c} \|Y^k - Y^{k+1}\|_2^2 < \infty. \quad (57)$$

By assumption (36), we have that the second term of the above inequality is bounded and $Y^{k+1} - Y^k \rightarrow 0$. Hence,

$$\sum_{k=0}^{\infty} c \|X^k - X^{k+1}\|_2^2 < \infty. \quad (58)$$

We may immediately obtain that $X^{k+1} - X^k \rightarrow 0$. \square

References

- [1] E.H. Land, J.J. McCann, Lightness and Retinex theory, *J. Opt. Soc. Am.* 61 (1) (1971) 1–11.
- [2] E.H. Land, The Retinex theory of color vision, *Sci. Am.* 237 (6) (1977) 108–128.

- [3] E.H. Land, Recent advances in Retinex theory and some implications for cortical computations: color vision and the natural image, *Proc Natl. Acad. Sci.* 80 (16) (1983) 5163–5169.
- [4] J.A. Frankle, J.J. McCann, Method and Apparatus for Lightness Imaging, United States Patent 4384336, May 17, 1983.
- [5] J. McCann, Lessons learned from Mondrians applied to real images and color gamuts., in: Proceedings of the IST/SID 7th Color Imaging Conference, 14, 1999, pp. 1–8.
- [6] B.V. Funt, F. Ciurea, J.J. McCann, Retinex in matlab, *J. Electr. Imaging* 13 (1) (2004) 48–57.
- [7] E.H. Land, An alternative technique for the computation of the designator in the Retinex theory of color vision, *Proc. Natl. Acad. Sci. U. S. Am.* 83 (10) (1986) 3078–3080.
- [8] B.K. Horn, Determining lightness from an image, *Graphical Models Graphical Models Image Process. Comput. Vis. Graphics Image Process.* 3 (4) (1974) 277–299.
- [9] J.M. Morel, A.B. Petro, C. Sbert, A PDE formalization of Retinex theory, *IEEE Trans. Image Process.* 19 (11) (2010) 2825–2837.
- [10] R. Kimmel, M. Elad, D. Shaked, R. Keshet, I. Sobel, A variational framework for Retinex, *Int. J. Comput. Vis.* 52 (1) (2003) 7–23.
- [11] W. Ma, S. Osher, A TV Bregman iterative model of Retinex theory, *Inverse Probl. Imaging* 6 (4) (2012) 697–708.
- [12] W. Ma, J.-M. Morel, S. Osher, A. Chien, An L1-based variational model for Retinex theory and its application to medical images, in: Proceedings of the IEEE Conference on Computer Vision and Pattern Recognition, 2011, pp. 153–160.
- [13] M.K. Ng, W. Wang, A total variation model for Retinex, *SIAM J. Imaging Sci.* 4 (1) (2011) 345–365.
- [14] W. Wang, C. He, A variational model with Barrier functionals for Retinex, *SIAM J. Imaging Sci.* 8 (3) (2015) 1955–1980.
- [15] X. Lan, H. Shen, L. Zhang, Q. Yuan, A spatially adaptive Retinex variational model for the uneven intensity correction of remote sensing images, *Signal Process.* 101 (2014) 19–34.
- [16] J. Liang, X. Zhang, Retinex by higher order total variation L^1 decomposition, *J. Math. Imaging Vis.* 52 (3) (2015) 345–355.
- [17] X. Fu, D. Zeng, Y. Huang, X.-P. Zhang, X. Ding, A weighted variational model for simultaneous reflectance and illumination estimation, in: Proceedings of the 2016 IEEE Conference on Computer Vision and Pattern Recognition (CVPR), 2016, pp. 2782–2790.
- [18] S. Park, S. Yu, B. Moon, S. Ko, J. Paik, Low-light image enhancement using variational optimization-based Retinex model, *IEEE Trans. Consum. Electr.* 63 (2) (2017) 178–184.
- [19] S. Boyd, N. Parikh, E. Chu, B. Peleato, J. Eckstein, Distributed optimization and statistical learning via the alternating direction method of multipliers, *Found. Trends Mach. Learn.* 3 (1) (2010) 1–122.
- [20] T. Goldstein, S. Osher, The split Bregman method for L1-regularized problems, *SIAM J. Imaging Sci.* 2 (2) (2009) 323–343.
- [21] Y. Xu, W. Yin, Z. Wen, Y. Zhang, An alternating direction algorithm for matrix completion with nonnegative factors, *Front. Math. China* 7 (2) (2012) 365–384.
- [22] A. Mittal, R. Soundararajan, A.C. Bovik, Making a completely blind image quality analyzer, *IEEE Signal Process. Lett.* 20 (2013) 209–212.
- [23] S. Wang, J. Zheng, H.-M. Hu, B. Li, Naturalness preserved enhancement algorithm for non-uniform illumination images, *IEEE Trans. Image Process.* 22 (2013) 3538–3548.
- [24] D. Martin, C. Fowlkes, D. Tal, J. Malik, A database of human segmented natural images and its application to evaluating segmentation algorithms and measuring ecological statistics, in: Proceedings of the IEEE International Conference on Computer Vision, 2, 2001, pp. 416–423 vol.2.
- [25] Z. Chen, T. Jiang, Y. Tian, Quality assessment for comparing image enhancement algorithms, in: Proceedings of the 2014 IEEE Conference on Computer Vision and Pattern Recognition CVPR '14, 2014, pp. 3003–3010.
- [26] K. He, J. Sun, X. Tang, Single image haze removal using dark channel prior, *IEEE Trans. Pattern Anal. Mach. Intell.* 33 (12) (2011) 2341–2353.